Supplementary Information

First-principles thermodynamic assessment of Sr-containing secondary phase formation in strontium-substituted lanthanum manganites for solid oxide cell applications

Yueh-Lin Lee[a,b]; Yuhua Duan[a]; Dan C. Sorescu[a]; Wissam A. Saidi[a]; Dane Morgan[c,d]; William Epting[e]; Harry Abernathy[c]*

[a]*National Energy Technology Laboratory, 626 Cochran Mill Road, Pittsburgh, PA 15236, USA*

[b]*NETL Support Contractor, 626 Cochran Mill Road, Pittsburgh, PA 15236, USA*

[c]*National Energy Technology Laboratory, 3610 Collins Ferry Road, Morgantown, WV 26505, USA*

[d]*Department of Materials Science and Engineering, University of Wisconsin–Madison, Madison, WI 53706, USA*

[d]*National Energy Technology Laboratory, 1450 SW Queen Ave, Albany, OR, 97321, USA*

[*] *Corresponding author: Yueh-Lin.Lee@netl.doe.gov*

Content:

Figure S 4. (a) The crystal structures of the rhombohedral $LaMnO_3$ (mp-19168) phase investigated in this work. (b) The calculated phonon dispersion of the rhombohedral $LaMnO_3$; the green and the purple profiles represent the phonon dispersions calculated at the harmonic approximation (HA) level and those calculated with the SCP method, respectively. (c) The vibrational free energy (F_vib) calculated at the quasi-harmonic approximation (QHA) level (green line) vs. that obtained from the self-consistent phonon (SCP) method (purple line). The orange line indicates the free energy difference between the two approaches. It is noted that there are some imaginary phonon modes (very small wiggles) close to the Γ point in the SCP phonon dispersions, potentially due to computational artifacts or complex interplay of electronic and lattice degrees of freedom[1]. As their impact is negligible, are neglected in the SCP vibrational free energy calculations.

Figure S 5. The simulated phonon dispersions of $La_{0.75}Sr_{0.25}MnO_3$ with various point defect species (a) V_A, (b) V_O, (c) V_B, (d) V_A-V_O (1NN), (e) (V_A&V_O) separated, and (f) S_O. The frequency unit in the y-axis is terahertz (THz).

Figure S 6. The calculated phonon dispersions of the Sr-secondary phases investigated in this work: (a) SrO (mp-2472), (b) $SrCO_3$ (mp-38035), (c) $SrSO_4$ (mp-5285), (d) $SrCrO_4$ (mp-510607), and (e) $Sr(OH_2)$ (mp-27425). The frequency unit in the y-axis is terahertz (THz).

Figure S 7. (a) The crystal structure, (b) the calculated ab initio free energies, (c) the simulated PBE+U phonon dispersions (U_{eff}=3.7 eV), and (d) the simulated PBE phonon dispersions of Cr_2O_3 (mp-19399). In (b), the solid blue circles are the data obtained from the National Institute of Standards and Technology (NIST) thermochemistry database.[1] The frequency unit in the y-axis is terahertz (THz) for (c) and (d).

Figure S 8. The calculated ab initio free energies of the gas molecules relative to their enthalpies at the standard condition for (a) O_2, (b) H_2O, (c) CO_2, (d) SO_2, (e) CrO_3, and (f) $CrO_2(OH)_2$. Both the PBE and PBE+U results are provided for CrO_3 and $CrO_2(OH)_2$. The solid blue circles are the data obtained from the NIST thermochemistry database[1], and the purple triangles in Figure S6(f) are the modeling results taken from Ref.[2].

Figure S 9. The calculated (orange circles) vs. experimental (green diamonds) equilibrium constants of the reactions[2] (a) $\frac{1}{2}\cdot Cr_2O_{3(s)} + \frac{3}{4}\cdot O_{2(g)} + H_2O_{(g)} \leftrightarrow + CrO_2(OH)_{2(g)}$*, and (b)* $\frac{1}{2}\cdot Cr_2O_{3(s)} + \frac{3}{4}\cdot O_{2(g)} \leftrightarrow CrO_{3(g)}$.

Figure S 10 The $V_A^{'''} - V_O^{\bullet\bullet}$ *defect structure of $La_{18}Sr_5Mn_{24}O_{71}$ (mp-19168) supercells investigated in this work: (a) first nearest neighbor (1NN)* $V_A^{'''} - V_O^{\bullet\bullet}$ *defect cluster, and (b) separated* $V_A^{'''}$ *and* $V_O^{\bullet\bullet}$ *with a pair distance of 9.8Å. The green, blue, purple, red, yellow, and grey spheres represent La, Sr, Mn, O,* $V_A^{'''}$*, and* $V_O^{\bullet\bullet}$*, respectively.*

Figure S 11. The calculated Brouwer diagrams of $(La_{0.8}Sr_{0.2})_{0.99}MnO_{3\pm\delta}$ bulk at (a) T= 873 K, (a) T= 973 K, and (c) T= 1173 K. The blue, orange, yellow, purple, green, pink, red, and black profiles refer to $V_A^{'''}$, $V_B^{'''}$, $Mn_B^{\bullet}$, $Mn_B^{'}$, Mn_B^{x}, $Mn_A^{'}$, $V_O^{\bullet}$, *and* La_A^{x}*, respectively. A slight deviation of A/B*

ratio from 1 to 0.99 is introduced to reduce the numerical instability in solving the defect model. The corresponding bulk defect thermodynamic parameters are provided in Table S 7 of SI.

Figure S 12. The calculated Brouwer diagrams of $(La_{0.8}Sr_{0.2})_{0.99}MnO_{3\pm\delta}$ (001) AO terminated surface at (a) T= 873 K, (b) T= 973 K, and (c) T= 1173 K. The blue, orange, yellow, purple, green, pink, red, and black profiles refer to $V_A^{'''}$, $V_B^{'''}$, $Mn_B^{\bullet}$, $Mn_B^{'}$, Mn_B^{x}, $Mn_A^{'}$, $V_O^{\bullet}$, and La_A^{x}, respectively. A slight deviation of A/B ratio from 1 to 0.99 is introduced to reduce the numerical instability in solving the defect model. The surface defect segregation energies reported in Table S 8, along with the bulk thermodynamic parameters of Table S 7, were used to generate the Brouwer diagram of the (001) AO terminated surface.

A. Notes on the defect calculations in the DFT modeling

- The atomic information of the defect simulations was summarized in Tables S1 and S2 of SI. There are no additional treatments used to extrapolate the defect energetics to the dilute limit, as the LSM materials can have substantial defect concentration that is much higher than the dilute scenario depending on the operating conditions.
- In the DFT modeling of this study, there were no further assessments to distinguish various charge states of point defect species. Defect formation was evaluated only with charge neutral supercell calculations where redistribution of the defect charge is allowed in the LSM supercells upon formation of a point defect. In the fully charge localized scenario, formation of $V_O^{\bullet\bullet}$ in the +2 charge state would simultaneously reduce two Mn^{3+} ions to form two Mn^{2+} ions, and in our DFT simulations, electron localization is treated automatically with the adopted DFT modeling method based on the selected functional.
- All simulations are performed using charge neutral supercell calculations where the charges generated upon formation of oxygen vacancies or cation vacancies are allowed to be redistributed in the LSM material, i.e., the generated defect charge is simultaneously coupled to change of the Fermi level or filling of the Mn 3d state and O 2p states in the defect containing supercells.
- Charge localization was treated with the adopted DFT+U with applications of the Hubbard U correction on the Mn 3d states (Refs. 18-19 of the main manuscript).
- The information of the Sr/La ratio in the DFT model was already provided in the Tables S1 and S2 of the SI.

Table S 1. Density functional theory and lattice dynamics modeling of the solid phases investigated in this study.

Solid Phase	**Reference and Label**
SrO	SrO (mp-2472)
Sr secondary phases	$SrCO_3$ (mp-38035) $SrSO_4$ (mp-5285) $SrCrO_4$ (mp-510607) $Sr(OH_2)$ (mp-27425)
Rhombohedral $LaMnO_3$ and $La0_{.75}Sr_{0.25}MnO_3$	$LaMnO_3$ ((mp-19168) $La_{18}Sr_6Mn_{24}O_{72}$ (perfect bulk) $La_{18}Sr_5Mn_{24}O_{72}$ ($1\,V_A'''$) $La_{18}Sr_6Mn_{23}O_{72}$ ($1\,V_B'''$) $La_{18}Sr_6Mn_{24}O_{71}$ ($1\,V_O^{\bullet\bullet}$) $La_{18}Sr_5Mn_{24}O_{71}$ ($1V_A'''$–$1V_O^{\bullet\bullet}$, first nearest neighbor) $La_{18}Sr_5Mn_{24}O_{71}$ ($1V_A'''$&$1V_O^{\bullet\bullet}$, separated)

Table S 2. The calculated phonon free energies of rhombohedral $La_{0.75}Sr_{0.25}MnO_3$ as a function of temperature.

Temperature (K)	$La_{0.75}Sr_{0.25}MnO_3$ (eV per FU)[a]	$La_{0.75}Sr_{0.208}MnO_3$ (eV per FU)	$La_{0.75}Sr_{0.25}M_{0.958}O_3$ (eV per FU)	$La_{0.75}Sr_{0.25}MnO_{2.958}$ (eV per FU)
DFT supercell	$La_{18}Sr_6Mn_{24}O_{72}$	$La_{18}Sr_5Mn_{24}O_{72}$	$La_{18}Sr_6Mn_{23}O_{72}$	$La_{18}Sr_6Mn_{24}O_{71}$
Label	bulk	V_A'''	V_B'''	$V_O^{\bullet\bullet}$
800	-0.8449	-0.8229	-0.8612	-0.8740
900	-1.0907	-1.0648	-1.1140	-1.1282
1000	-1.3506	-1.3207	-1.3814	-1.3970
1100	-1.6232	-1.5893	-1.6620	-1.6790
1200	-1.9074	-1.8693	-1.9546	-1.9730

Temperature (K)	$La_{0.75}Sr_{0.25}MnO_3$ (eV per FU)	$La_{0.75}Sr_{0.208}MnO_3$ (eV per FU)
DFT supercell	$La_{18}Sr_5Mn_{24}O_{71}$	$La_{18}Sr_5Mn_{24}O_{71}$
Label	$1NN\ V_A''' - V_O^{\bullet\bullet}$	Separated $V_A''' - V_O^{\bullet\bullet}$
800	-0.8164	-0.8266
900	-1.0563	-1.0678
1000	-1.3100	-1.3228
1100	-1.5762	-1.5904
1200	-1.8539	-1.8693

[a] The calculated phonon energies at T=300 K for $La_{0.75}Sr_{0.25}MnO_3$ bulk is 0.446 eV/FU.

Table S 3. The calculated phonon free energies of the Sr oxide and Sr secondary phases as a function of temperature.

T (K)	*SrO* (eV per FU)	$SrCO_3$ (eV per FU)	$SrSO_4$ (eV per FU)	$SrCrO_4$ (eV per FU)	$Sr(OH)_2$ (eV per FU)
800	-0.4447	-0.6038	-0.7782	-0.7782	-0.2044
900	-0.5557	-0.8298	-1.0519	-1.0519	-0.4094
1000	-0.6725	-1.0690	-1.3418	-1.3418	-0.6266
1100	-0.7944	-1.3201	-1.6463	-1.6463	-0.8549
1200	-0.9210	-1.5823	-1.9643	-1.9643	-1.0935

[a]The calculated phonon energies at T=300 K for *SrO*, $SrCO_3$, $SrSO_4$, $SrCrO_4$, and $Sr(OH)_2$ are –0.008, 0.628, 0.692, 0.627, and 0.880 eV/FU, respectively.

Table S 4. The calculated zero-point energies of the gas phase molecules.

Gas Molecule Type	Zero-point energy, eV/molecule
O_2	0.098
SO_2	0.178
CO_2	0.309
H_2O	0.569
CrO_3	0.236 (0.231, GGA+U)
$CrO_2(OH)_2$	0.909 (0.920, GGA+U)

Table S 5. The calculated free energies of the gas phase molecules as a function of temperature.

T (K)	$O_{2(gas)}$ (eV)	$SO_{2(gas)}$ (eV)	$CO_{2(gas)}$ (eV)	$H_2O_{(gas)}$ (eV)	$CrO_{3(gas)}$ (eV)	$CrO_2(OH)_{2(gas)}$ (eV)
800	-0.8959	-2.1906	-1.8987	-1.6691	-2.4004	-2.3465
900	-1.0195	-2.4980	-2.1687	-1.9038	-2.7508	-2.8641
1000	-1.1447	-2.8118	-2.4449	-2.1423	-3.1093	-3.3972
1100	-1.2718	-3.1318	-2.7271	-2.3862	-3.4761	-3.9445
1200	-1.4004	-3.4563	-3.0135	-2.6330	-3.8518	-4.5048

Table S 6. The thermodynamic parameters of the defect reactions used in the defect modeling. These parameters are used to determine the equilibrium constants of the O vacancy formation (Eq [T1.7b]), Charge disproportionation reaction (Eq [T1.8b]), Schottky defect formation (Eq [T1.9b]), and $Mn_A^{'}$ antisite formation (Eq [T1.10b]) as listed in Table 1 of the main manuscript.

	Reaction energy, eV	**Reaction entropy, meV/K**
O vacancy formation	2.85	0.83
Charge disproportion reaction	0.10	0.01
Schottky Defect Formation	6.75	0.02
$Mn_A^{'}$ **antisite formation**	0.90	0.00

Table S 7. The calculated $La_{18}Sr_6Mn_{24}O_{72}$ (001) AO surface defect segregation and the oxygen surface adsorption energies.

Defect Label	Defect Surface Segregation Energy, eV
$V_A^{'''}(Sr) - V_O^{\bullet\bullet}$(1NN)	-1.67
$V_A^{'''}(Sr) - V_O^{\bullet\bullet}$(Far)	-1.09
$V_A^{'''}$(Sr)	-2.21
$V_A^{'''}$(La)	-2.37
$V_B^{'''}$(Mn)	-1.24
$V_O^{\bullet\bullet}$(Top layer)	0.78
$V_O^{\bullet\bullet}$(Second layer)	0.89
Label	Surface O Adsorption Energy, eV
$O_{ad}^{''}(001)_{AO}$	-0.7 ~ -1.3 eV/O (among 6 configurations)

Table S 8. List of SrO formation reactions included in this study that are coupled to the LSM point defect equilibria.

Reaction Free Energy Label	**Summary of Reaction Step 1 Expressions for *SrO* Formation from *LSM***
	1. $La_{18}Sr_6Mn_{24}O_{72}$+1/2·$O_{2(g)}$↔$La_{18}Sr_5Mn_{24}O_{72}$+SrO
$\Delta G_{SrO\ form\ 1}^{ab\ initio}$	$2\left[Mn_B^x\right]+\left[Sr_A^{'}\right]+1/2\cdot O_{2(g)} \leftrightarrow 2\left[Mn_B^{\bullet}\right]+\left[V_A^{'''}\right]+SrO_{(s)}$ DFT Model: $La_{18}Sr_6Mn_{24}O_{72}+1/2\cdot O_{2(g)} \leftrightarrow La_{18}Sr_5Mn_{24}O_{72}\,(V_A^{'''})+SrO$
	$K_{SrO\ form\ 1}^{eq}=\frac{\left[Mn_B^{\bullet}\right]^2\cdot\left[V_A^{'''}\right]\cdot[SrO_{(s)}]}{\left[Mn_B^x\right]^2\left[Sr_A^{'}\right]p(O_2)^{0.5}}=exp(\frac{-\Delta G_{SrO\ form\ 1}^{ab\ initio}}{k_bT})$ $[SrO_{(s)}]=K_{eq}\frac{\left[Mn_B^x\right]^2\cdot\left[Sr_A^{'}\right]\cdot p(O_2)^{0.5}}{\left[Mn_B^{\bullet}\right]^2\cdot\left[V_A^{'''}\right]}$
	1a & 1b. $La_{18}Sr_6Mn_{24}O_{72}$↔$La_{18}Sr_5Mn_{24}O_{71}$+SrO
$\Delta G_{SrO\ form\ 1a}^{ab\ initio}$	(1a) $\left[Sr_A^{'}\right]+\left[O_O^x\right]\leftrightarrow\left[V_A^{'''}\right]+\left[V_O^{\bullet\bullet}\right]+SrO_{(s)}$ DFT Model: $La_{18}Sr_6Mn_{24}O_{72} \leftrightarrow La_{18}Sr_5Mn_{24}O_{71}\,(separated\ V_A^{'''}\&\ V_O^{\bullet\bullet})+SrO$
	$K_{SrO\ form\ 1a}^{eq}=\frac{\left[V_A^{'''}\right]\cdot\left[V_O^{\bullet\bullet}\right]\cdot[SrO_{(s)}]}{\left[Sr_A^{'}\right]\cdot\left[O_O^x\right]}=exp(\frac{-\Delta G_{SrO\ form\ 1a}^{ab\ initio}}{k_bT})$ $[SrO_{(s)}]=K_{eq}\frac{\left[Sr_A^{'}\right]\left[O_O^x\right]}{\left[V_A^{'''}\right]\cdot\left[V_O^{\bullet\bullet}\right]}$
$\Delta G_{SrO\ form\ 1b}^{ab\ initio}$	(1b) $\left[Sr_A^{'}\right]+\left[O_O^x\right]\leftrightarrow\left[V_A^{'''}-V_O^{\bullet\bullet}\right]+SrO_{(s)}$ DFT Model: $La_{18}Sr_6Mn_{24}O_{72} \leftrightarrow La_{18}Sr_5Mn_{24}O_{71}\,(^{1NN}V_A^{'''}-V_O^{\bullet\bullet})+SrO$
	$K_{SrO\ form\ 1b}^{eq}=\frac{\left[V_A^{'''}-V_O^{\bullet\bullet}\right]\cdot[SrO_{(s)}]}{\left[Sr_A^{'}\right]\cdot\left[O_O^x\right]}=exp(\frac{-\Delta G_{SrO\ form\ 1b}^{ab\ initio}}{k_bT})$ $[SrO_{(s)}]=K_{eq}\frac{\left[Sr_A^{'}\right]\left[O_O^x\right]}{\left[V_A^{'''}-V_O^{\bullet\bullet}\right]}$

Table S 9. The calculated vibrational free energies of the adsorbed O_{ad} on the $La_{18}Sr_6Mn_{24}O_{72}$ (001) AO terminated surface. Two O_{ad} configurations were included in the table to present the upper and lower energy configurations among the six investigated surface O_{ad}s.

	eV	**eV**
Temp (K)	O_{ad} Conf_1	O_{ad} Conf_3
0	0.06534	0.06501
300	0.04735	0.04693
473	0.01019	0.00963
673	-0.05121	-0.05196
773	-0.08769	-0.08854
873	-0.12740	-0.12835
973	-0.16999	-0.17104
1073	-0.21518	-0.21634
1173	-0.262739	-0.26400

(a) *SrO* (mp-2472)

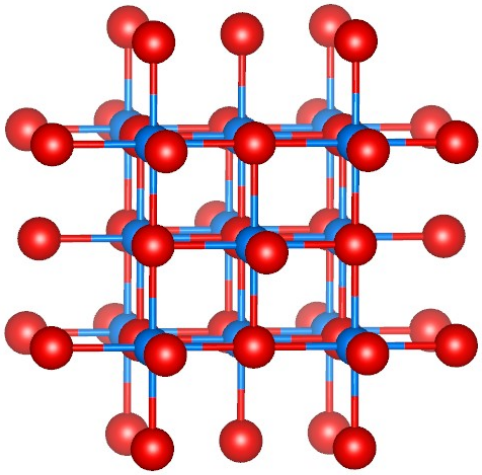

(b) $SrCO_3$ (mp-38035)

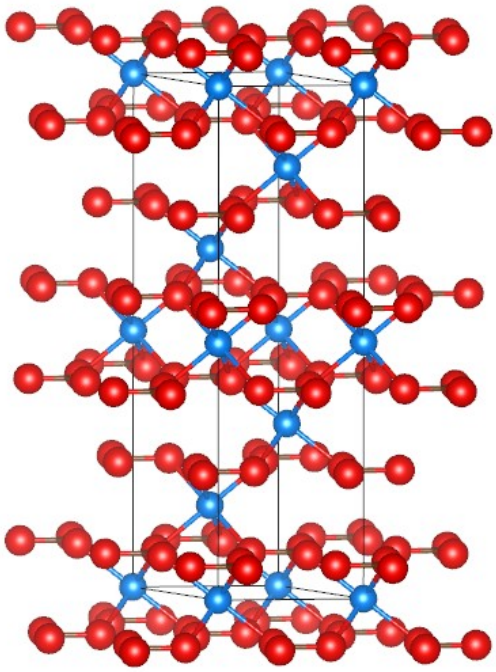

(c) $SrSO_4$ (mp-5285)

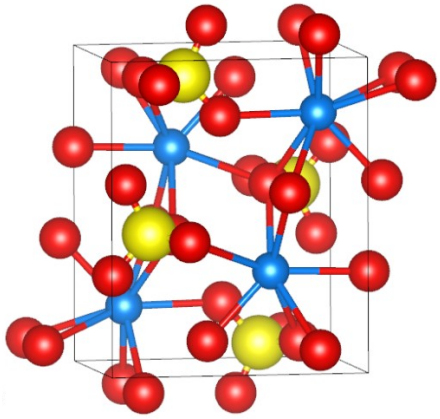

(d) $SrCrO_4$ (mp-510607)

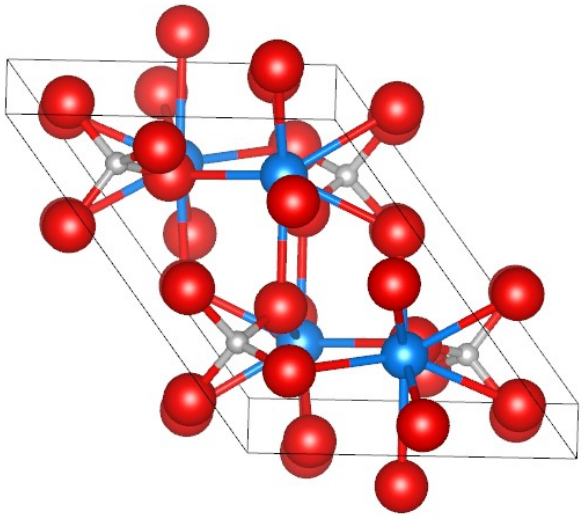

(e) $Sr(OH_2)$ (mp-27425)

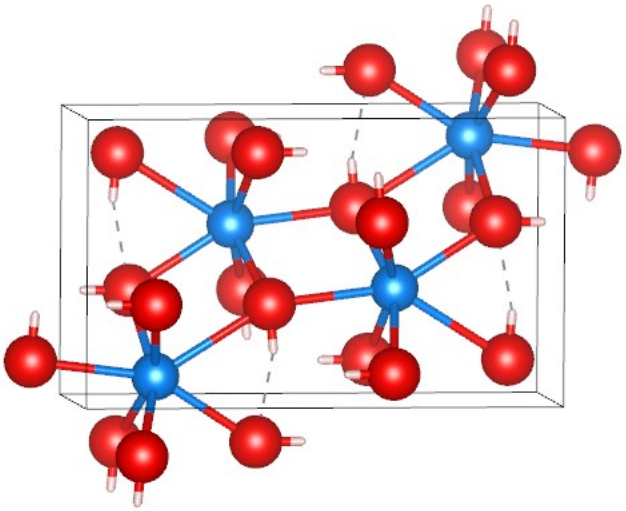

Figure S 1. The crystal structures of the Sr-related solid-phases investigated in this work, including (a) SrO (mp-2472, (b) $SrCO_3$ (mp-38035), (c) $SrSO_4$ (mp-5285), (d) $SrCrO_4$ (mp-510607), and (e) $Sr(OH_2)$ (mp-27425). The blue, red, brown, yellow, grey, and pink spheres represent Sr, O, C, S, Cr, and H atoms, respectively.

(a) *$LaMnO_3$* (mp-19168)

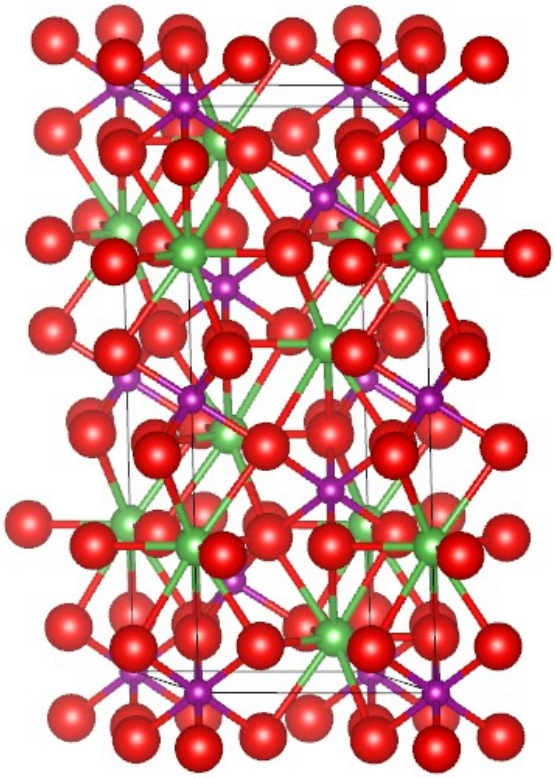

(b) $La_{0.75}Sr_{0.25}MnO_3$ supercell created based on $LaMnO_3$ (mp-19168)
a = 11.07102 Å
b = 9.64788 Å
c = 13.40843 Å
α = 89.5867°
β = 90.0000°
γ = 90.0000°

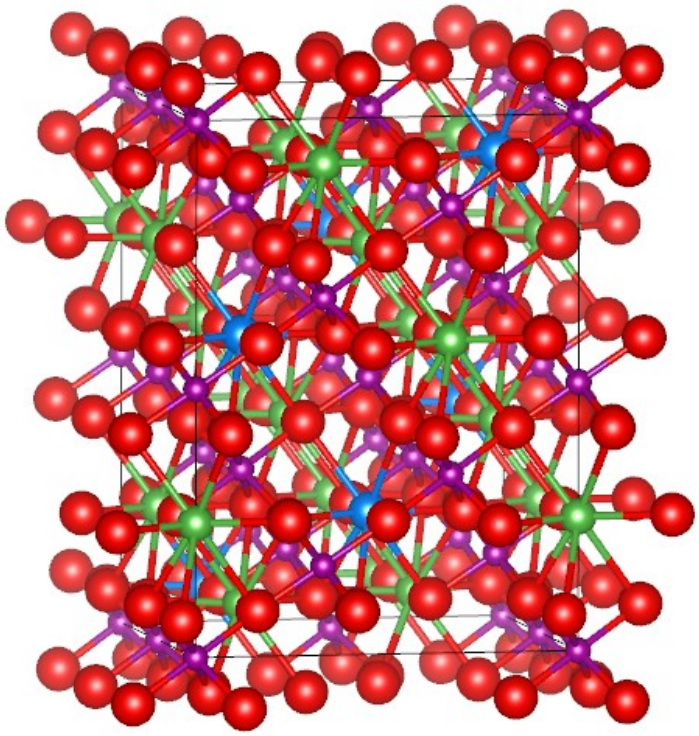

Figure S 2. The crystal structures of (a) $LaMnO_3$ (mp-19168) and (b) $La_{0.75}Sr_{0.25}MnO_3$ supercell (a 120-atom supercell of $La_{18}Sr_6Mn_{24}O_{72}$). The green, blue, purple, and red spheres represent La, Sr, Mn, and O atoms, respectively.

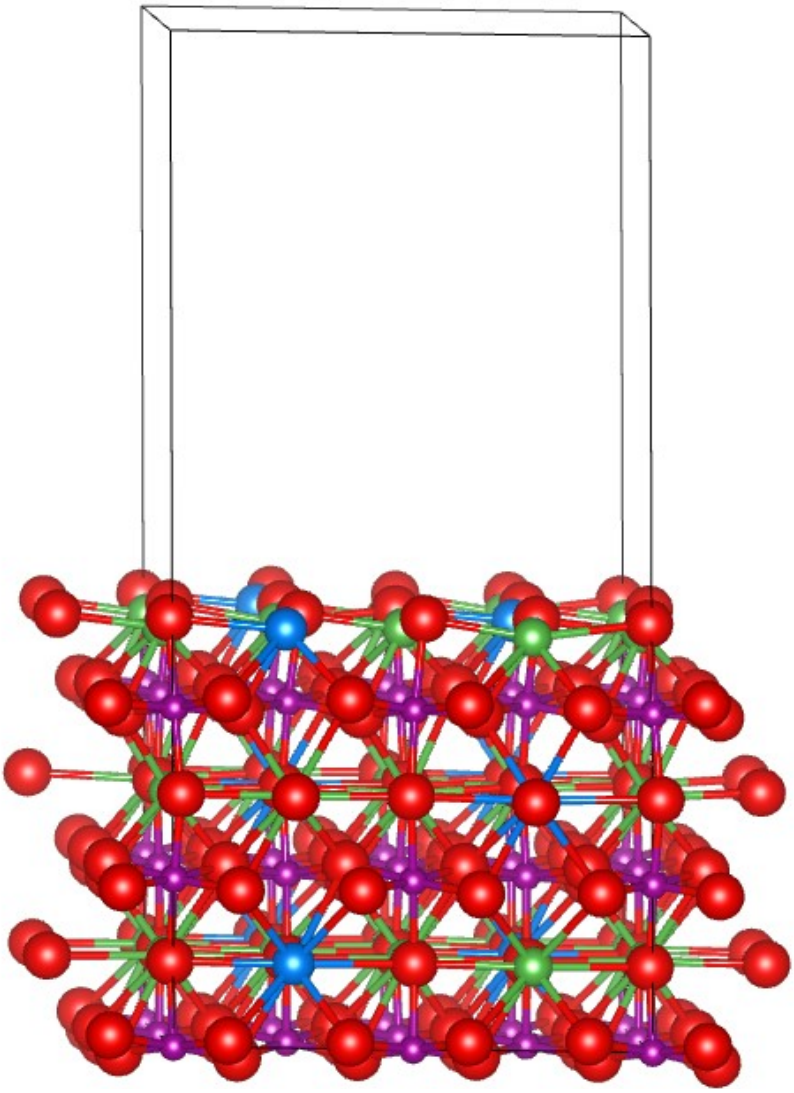

Figure S 3. The (001) AO terminated $La_{18}Sr_6Mn_{24}O_{72}$ slab model used for modeling the surface defect energetics reported in Table S8. The green, blue, purple, and red spheres represent La, Sr, Mn, and O atoms, respectively. In this slab model, the bottom two slab layers are fixed to the coordinates of bulk rhombohedral $La_{0.75}Sr_{0.25}MnO_3$ (created based on the rhombohedral $LaMnO_3$ phase; mp-19168), whereas the point defects are placed at the top two surface layers.

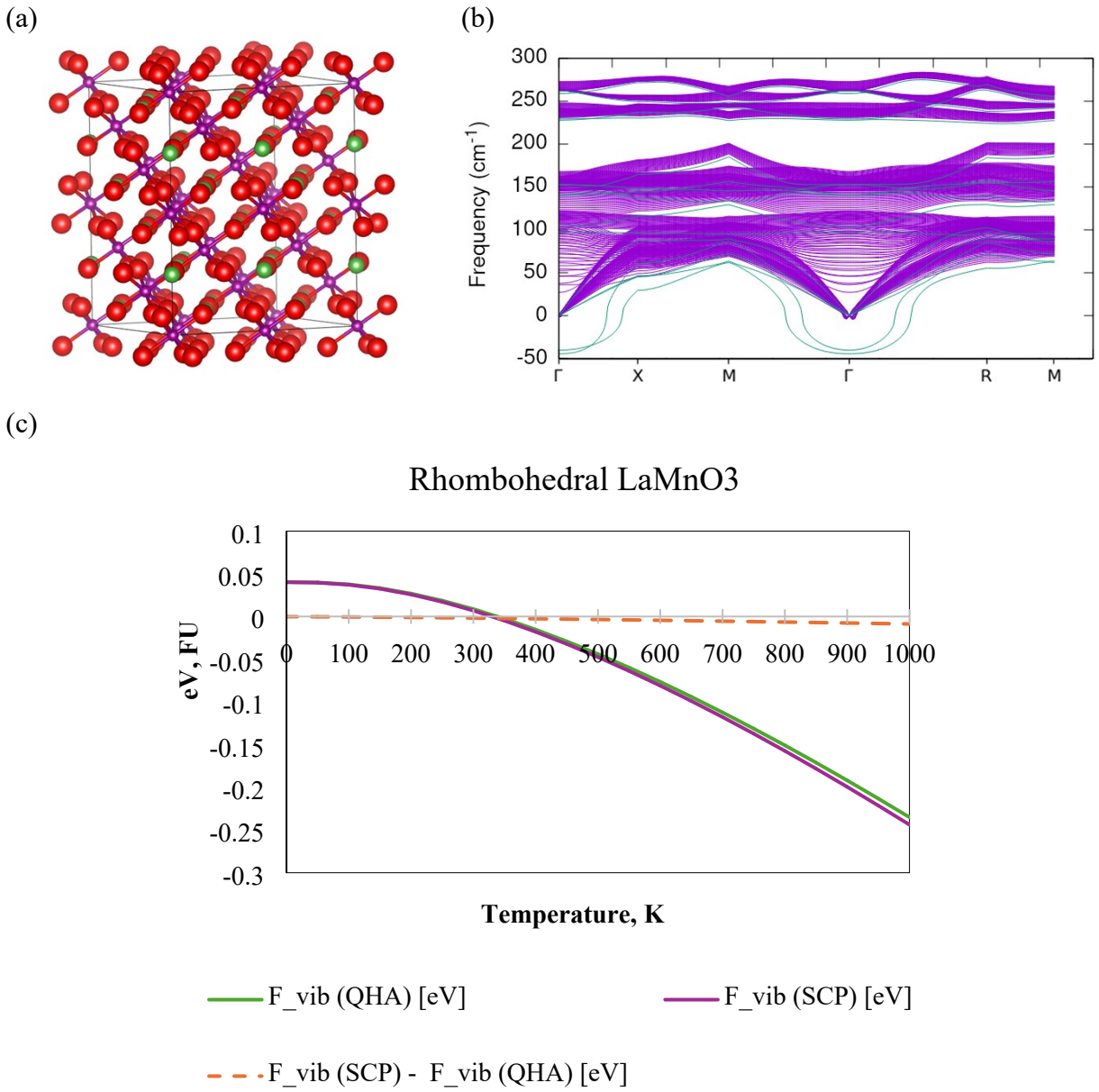

Figure S 4. (a) The crystal structures of the rhombohedral $LaMnO_3$ (mp-19168) phase investigated in this work. (b) The calculated phonon dispersion of the rhombohedral $LaMnO_3$; the green and the purple profiles represent the phonon dispersions calculated at the harmonic approximation (HA) level and those calculated with the SCP method, respectively. (c) The vibrational free energy (F_vib) calculated at the quasi-harmonic approximation (QHA) level (green line) vs. that obtained from the self-consistent phonon (SCP) method (purple line). The orange line indicates the free energy difference between the two approaches. It is noted that there are some imaginary phonon modes (very small wiggles) close to the Γ point in the SCP phonon dispersions, potentially due to computational artifacts or complex interplay of electronic and lattice degrees of freedom[1]. As their impact is negligible, are neglected in the SCP vibrational free energy calculations.

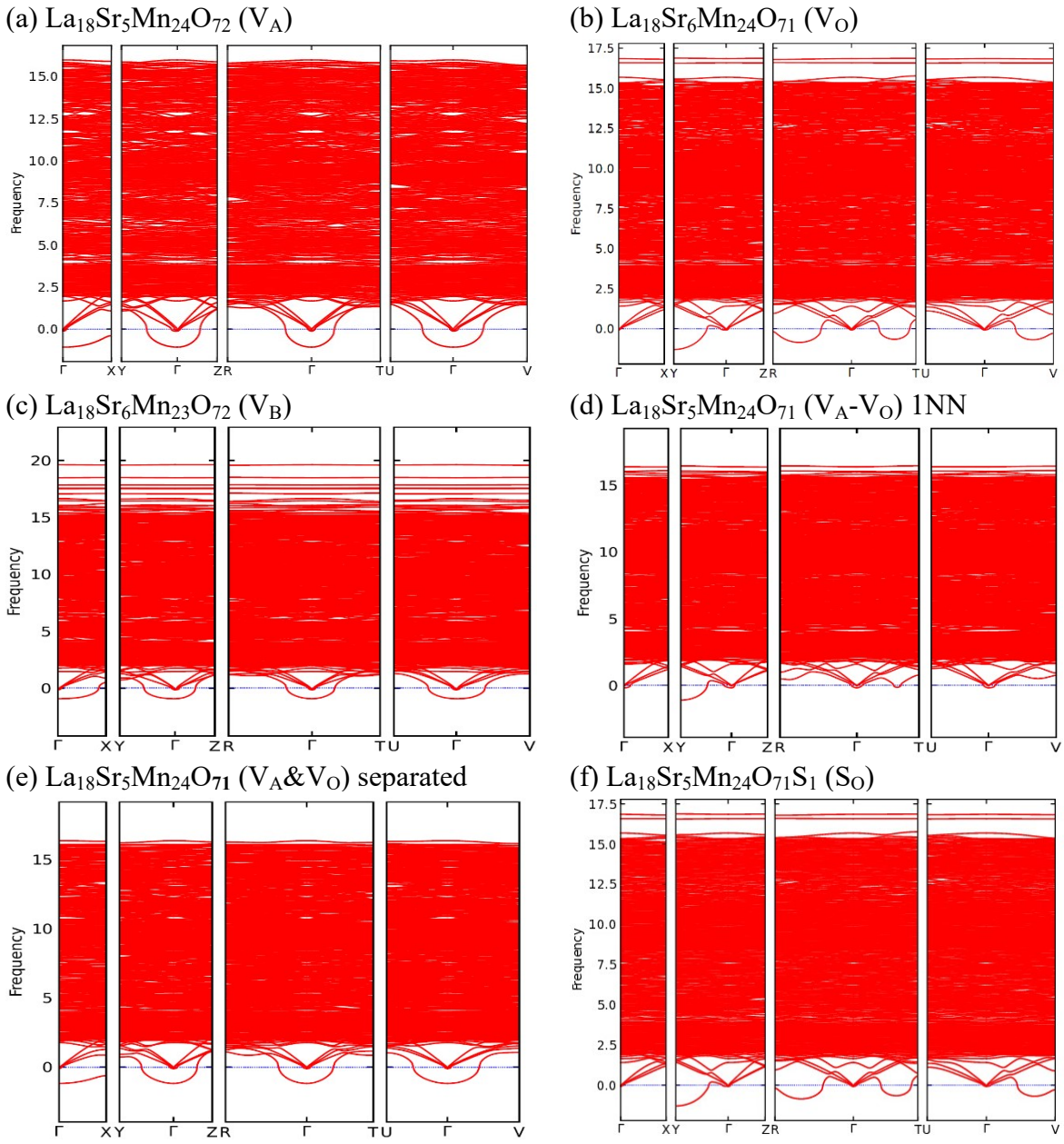

Figure S 5. The simulated phonon dispersions of $La_{0.75}Sr_{0.25}MnO_3$ with various point defect species (a) V_A, (b) V_O, (c) V_B, (d) V_A-V_O (1NN), (e) (V_A&V_O) separated, and (f) S_O. The frequency unit in the y-axis is terahertz (THz).

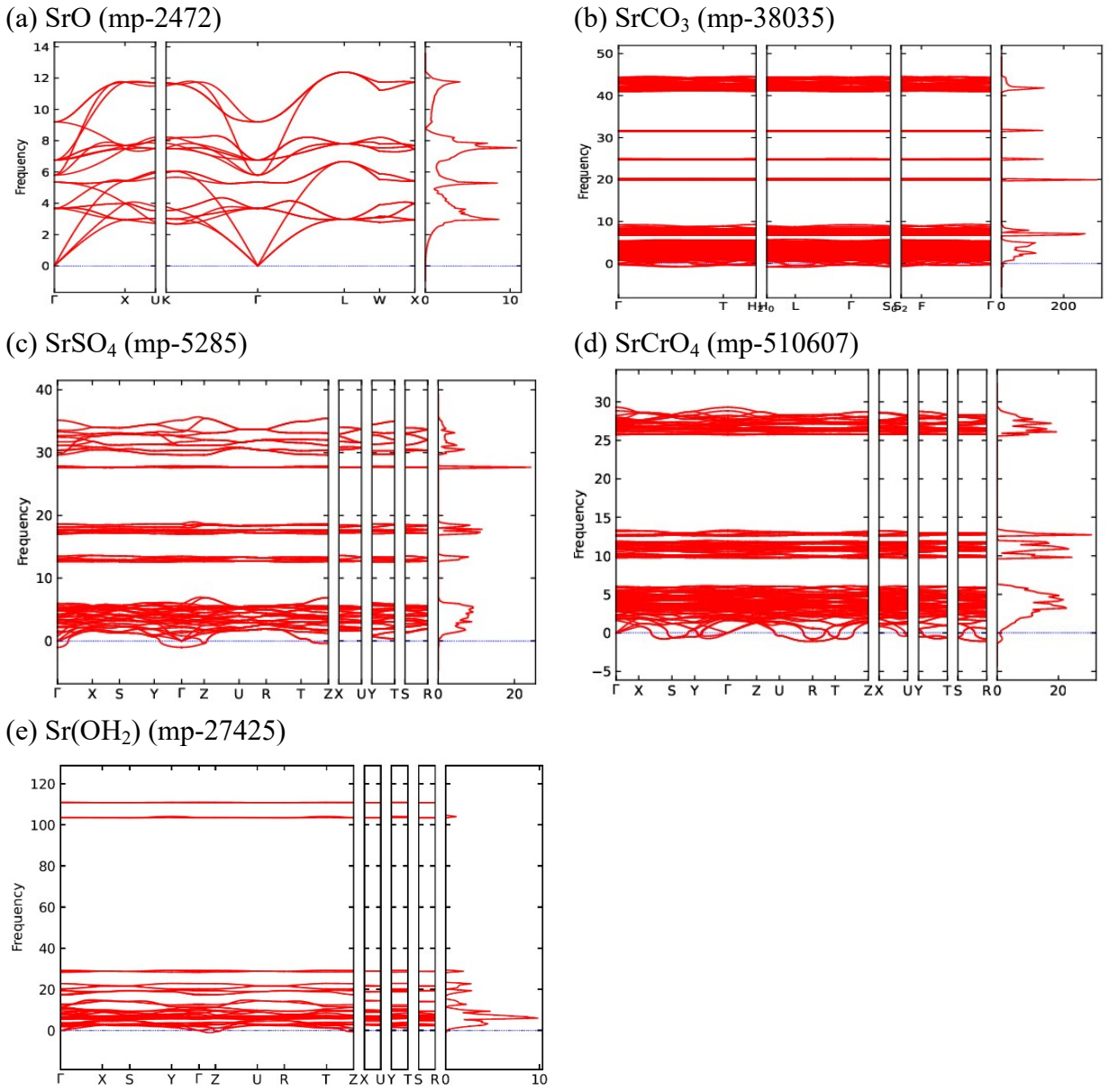

Figure S 6. The calculated phonon dispersions of the Sr-secondary phases investigated in this work: (a) SrO (mp-2472), (b) $SrCO_3$ (mp-38035), (c) $SrSO_4$ (mp-5285), (d) $SrCrO_4$ (mp-510607), and (e) $Sr(OH_2)$ (mp-27425). The frequency unit in the y-axis is terahertz (THz).

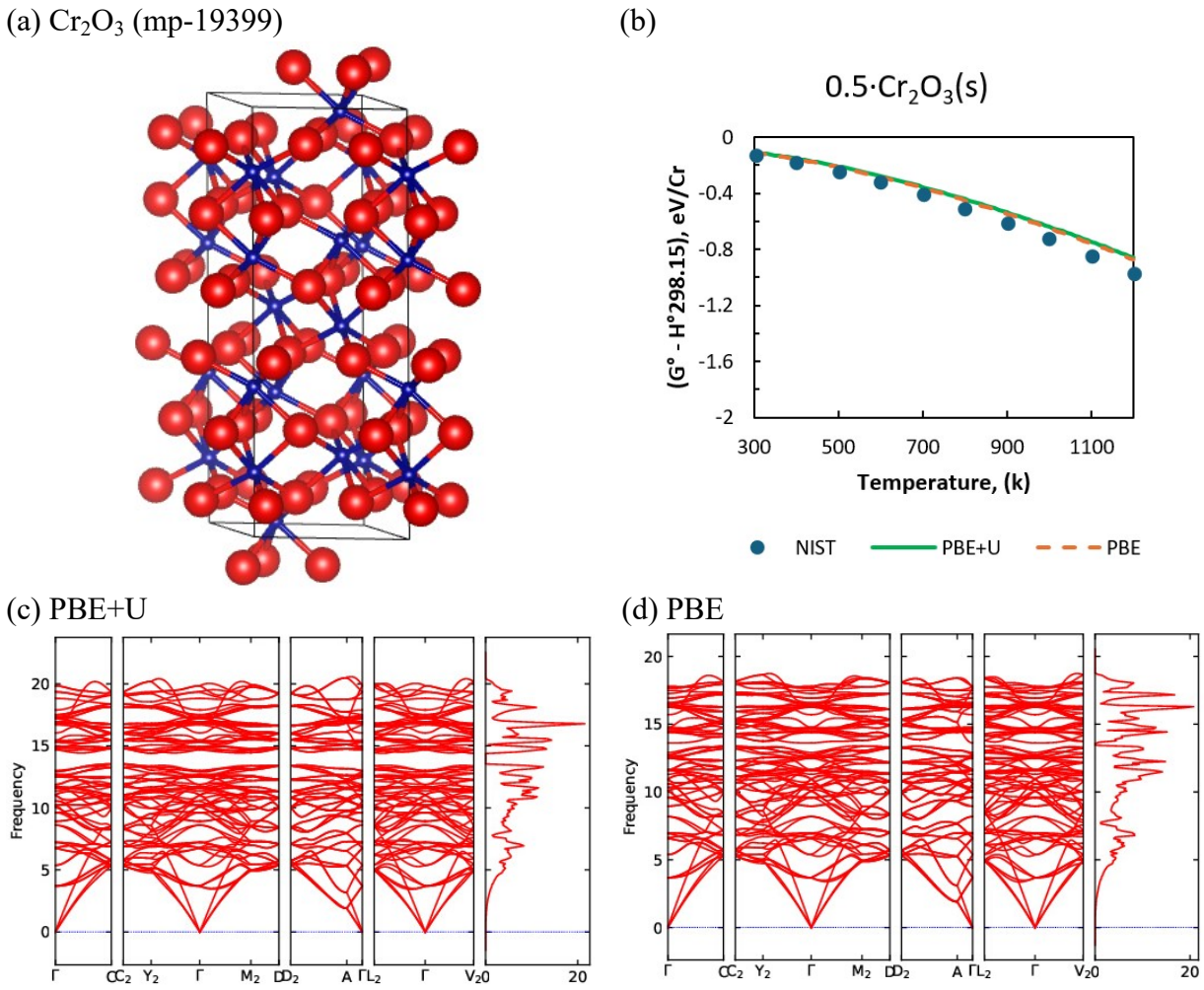

Figure S 7. (a) The crystal structure, (b) the calculated ab initio free energies, (c) the simulated PBE+U phonon dispersions (U_{eff}=3.7 eV), and (d) the simulated PBE phonon dispersions of Cr_2O_3 (mp-19399). In (b), the solid blue circles are the data obtained from the National Institute of Standards and Technology (NIST) thermochemistry database.[2] The frequency unit in the y-axis is terahertz (THz) for (c) and (d).

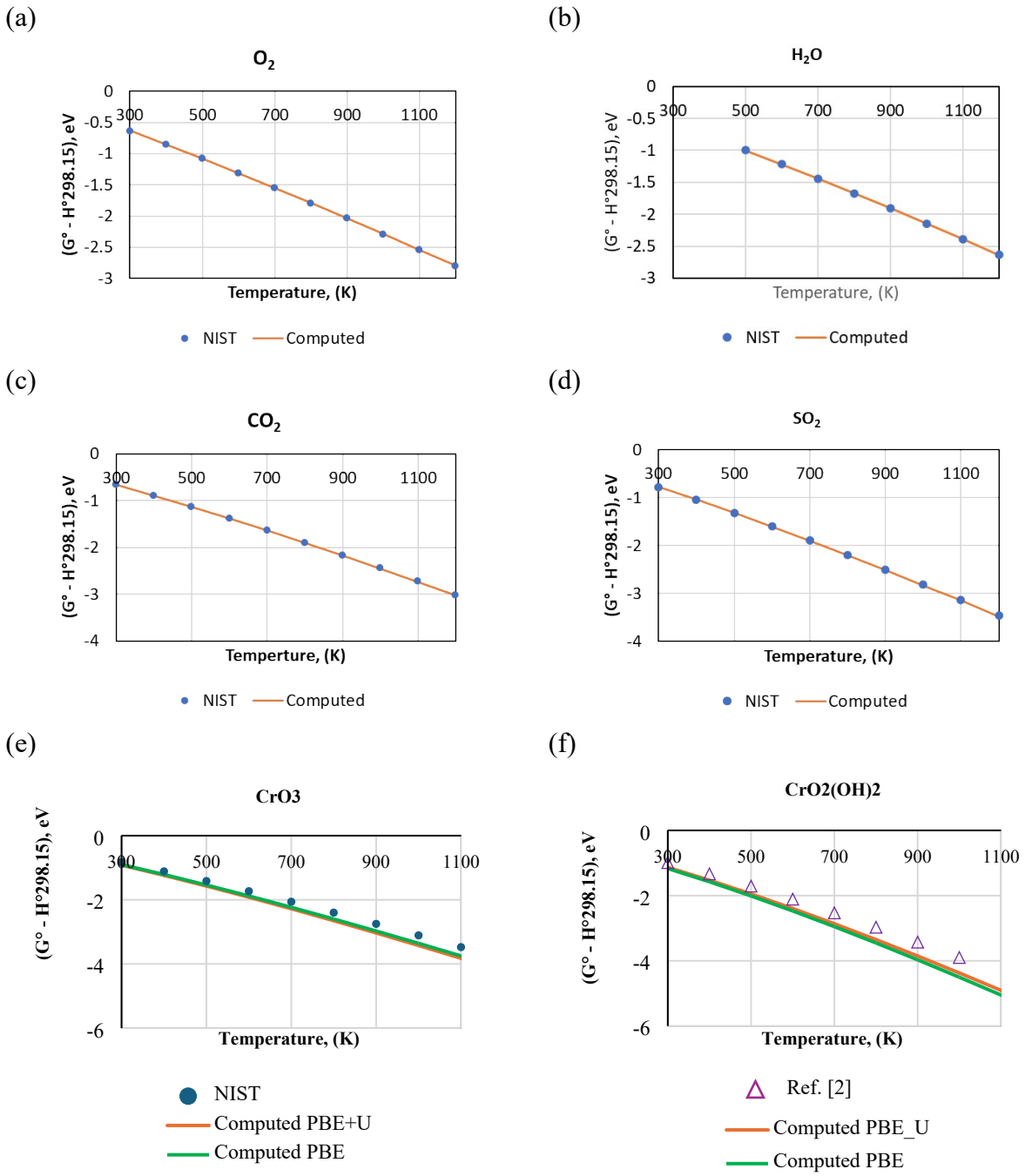

Figure S 8. The calculated ab initio free energies of the gas molecules relative to their enthalpies at the standard condition for (a) O_2, (b) H_2O, (c) CO_2, (d) SO_2, (e) CrO_3, and (f) $CrO_2(OH)_2$. Both the PBE and PBE+U results are provided for CrO_3 and $CrO_2(OH)_2$. The solid blue circles are the data obtained from the NIST thermochemistry database[2], and the purple triangles in Figure S6(f) are the modeling results taken from Ref.3.

(a) $\frac{1}{2}\cdot Cr_2O_{3(s)}+\frac{3}{4}\cdot O_{2(g)}+H_2O_{(g)}\leftrightarrow+CrO_2(OH)_{2(g)}$

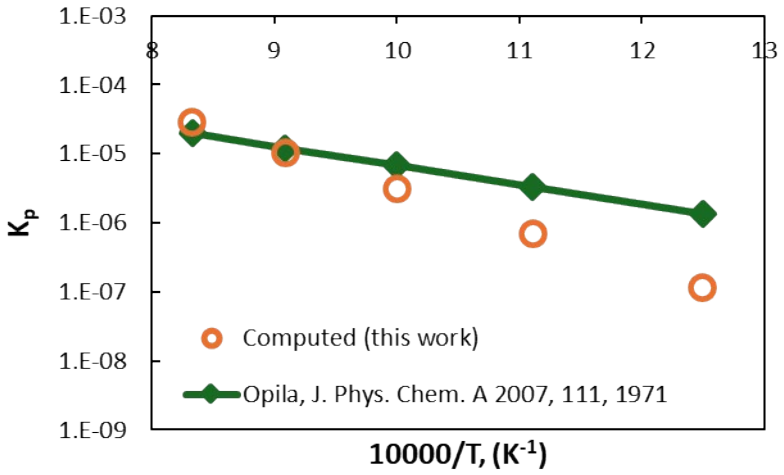

(b) $\frac{1}{2}\cdot Cr_2O_{3(s)}+\frac{3}{4}\cdot O_{2(g)}\leftrightarrow CrO_{3(g)}$

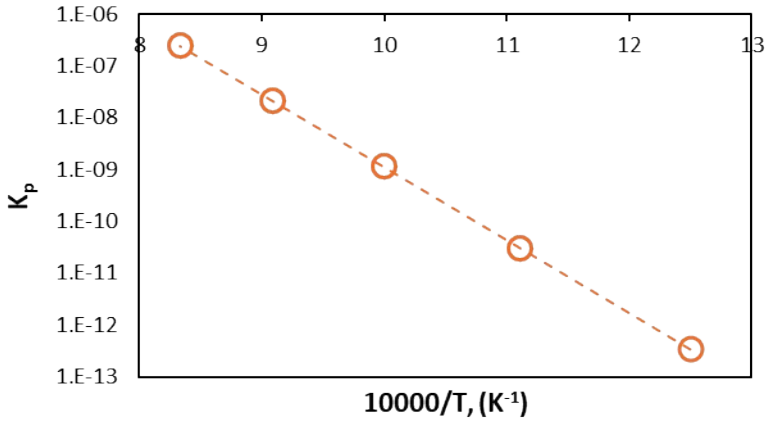

Figure S 9. The calculated (orange circles) vs. experimental (green diamonds) equilibrium constants of the reactions[2] (a) $\frac{1}{2}\cdot Cr_2O_{3(s)}+\frac{3}{4}\cdot O_{2(g)}+H_2O_{(g)}\leftrightarrow+CrO_2(OH)_{2(g)}$*, and (b)* $\frac{1}{2}\cdot Cr_2O_{3(s)}+\frac{3}{4}\cdot O_{2(g)}\leftrightarrow CrO_{3(g)}$.

(a) 1NN $V_A^{'''} - V_O^{\bullet\bullet}$

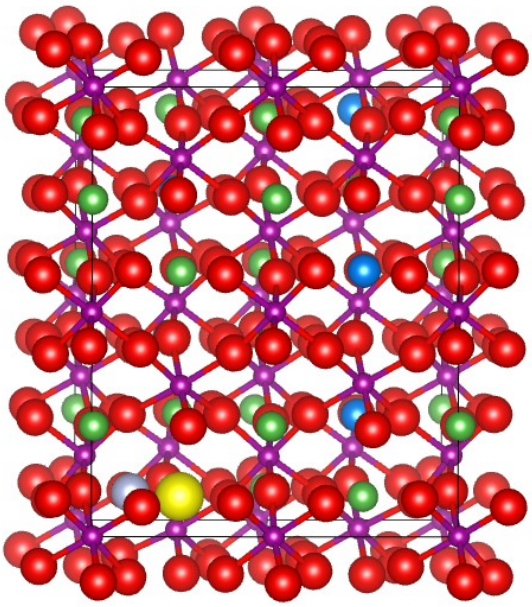

(b) Separated $V_A^{'''}$ and $V_O^{\bullet\bullet}$

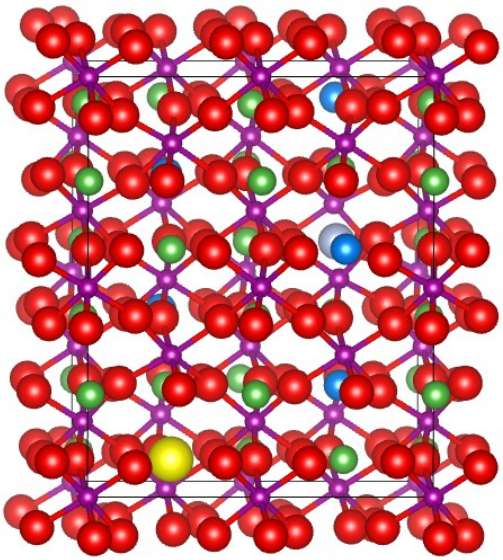

Figure S 10. The $V_A^{'''} - V_O^{\bullet\bullet}$ defect structure of La18Sr5Mn24O71 (mp-19168) supercells investigated in this work: (a) first nearest neighbor (1NN) $V_A^{'''} - V_O^{\bullet\bullet}$ defect cluster, and (b) separated $V_A^{'''}$ and $V_O^{\bullet\bullet}$ with a pair distance of 9.8Å. The green, blue, purple, red, yellow, and grey spheres represent La, Sr, Mn, O, $V_A^{'''}$, and $V_O^{\bullet\bullet}$, respectively.

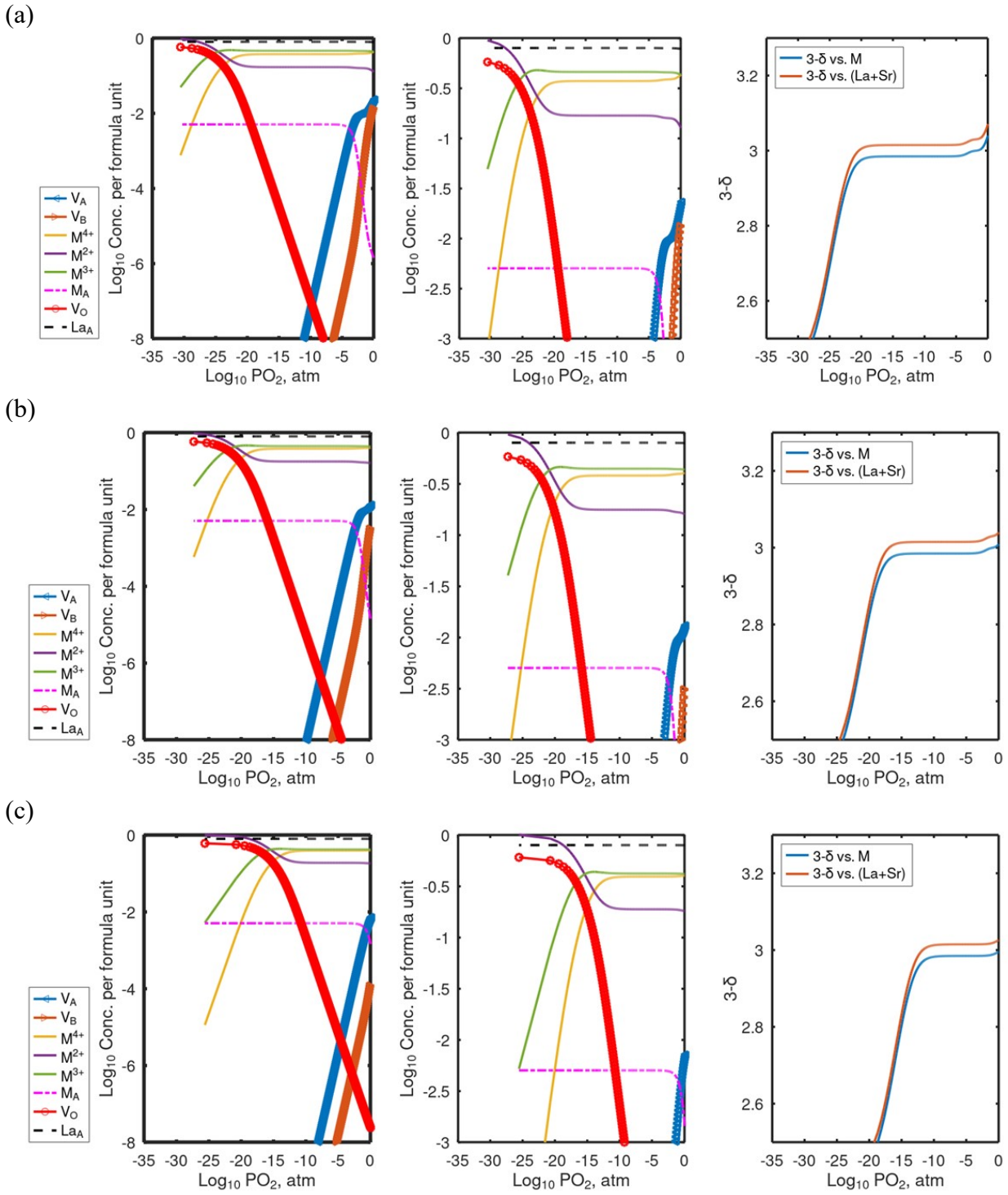

Figure S 11. The calculated Brouwer diagrams of $(La_{0.8}Sr_{0.2})_{0.99}MnO_{3\pm\delta}$ bulk at (a) T= 873 K, (a) T= 973 K, and (c) T= 1173 K. The blue, orange, yellow, purple, green, pink, red, and black profiles refer to V_A''', V_B''', $Mn_B^{\bullet}$, Mn_B', Mn_B^x, Mn_A', $V_O^{\bullet}$, and La_A^x, respectively. A slight deviation of A/B ratio from 1 to 0.99 is introduced to reduce the numerical instability in solving the defect model. The corresponding bulk defect thermodynamic parameters are provided in Table S 7 of SI.

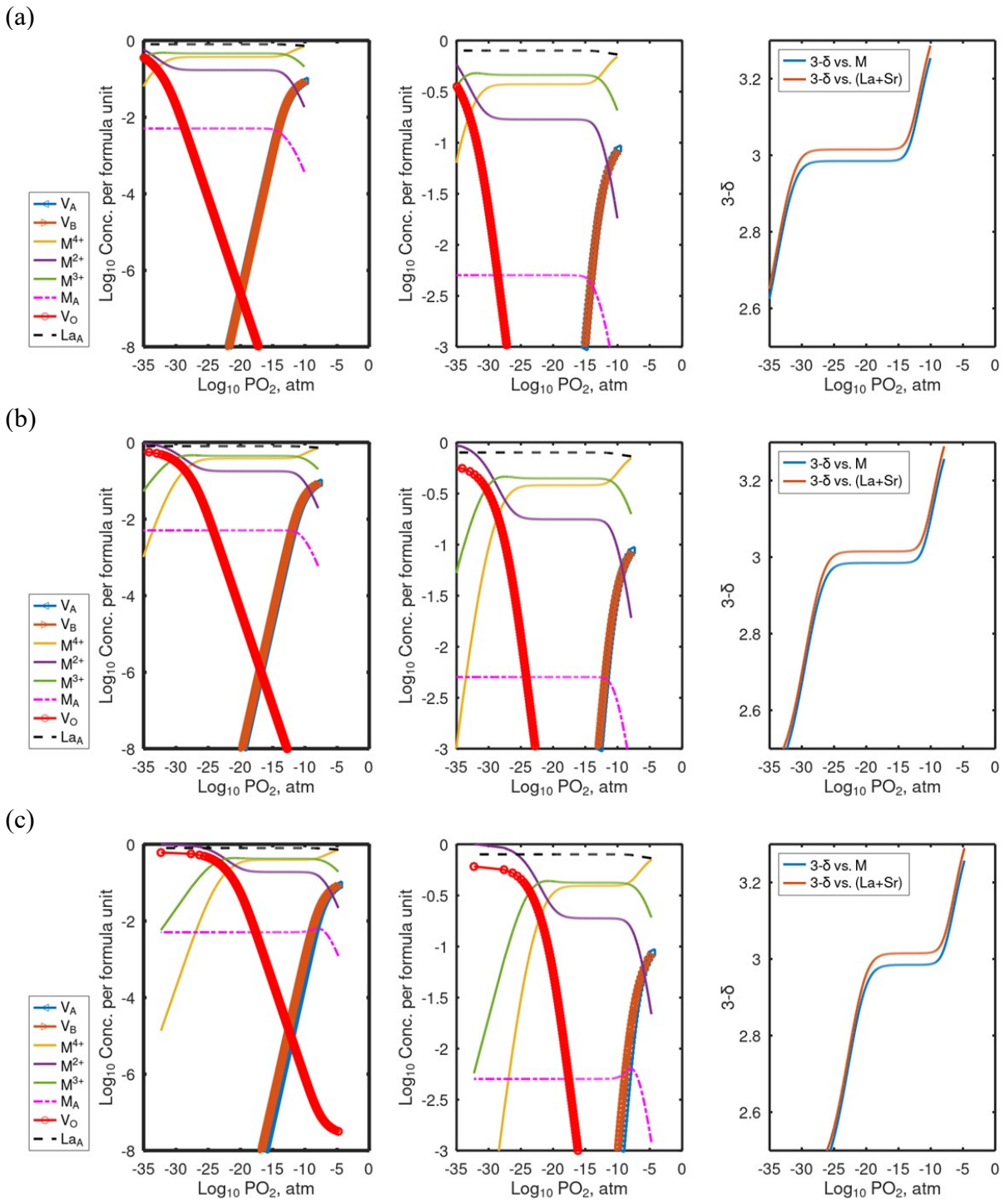

Figure S 12. The calculated Brouwer diagrams of $(La_{0.8}Sr_{0.2})_{0.99}MnO_{3\pm\delta}$ (001) AO terminated surface at (a) T= 873 K, (b) T= 973 K, and (c) T= 1173 K. The blue, orange, yellow, purple, green, pink, red, and black profiles refer to V_A''', V_B''', $Mn_B^{\bullet}$, Mn_B', Mn_B^x, Mn_A, $V_O^{\bullet}$, and La_A^x, respectively. A slight deviation of A/B ratio from 1 to 0.99 is introduced to reduce the numerical instability in solving the defect model. The surface defect segregation energies reported in Table S 8, along with the bulk thermodynamic parameters of Table S 7, were used to generate the Brouwer diagram of the (001) AO terminated surface.

References:

1. M. M. Schmitt, Y. Zhang, A. Mercy and P. Ghosez, *Physical Review B*, 2020, **101**, 21430.
2. P. Linstorm, Journal of Physical and Chemical Reference Data Monographs or Supplements, 1998, 9, 1-1951.
3. E. J. Opila, D. L. Myers, N. S. Jacobson, I. M. B. Nielsen, D. F. Johnson, J. K. Olminsky and M. D. Allendorf, The Journal of Physical Chemistry A, 2007, 111, 1971-1980.